JOURNAL OF GEOPHYSICAL RESEARCH, VOL. 112, D13312, doi:10.1029/2006JD008077, 2007

Click Here for Full Article

"Designing Lagrangian experiments to measure regional-scale trace gas fluxes"

J. C. Lin,[1] C. Gerbig,[2] S. C. Wofsy,[3] V. Y. Chow,[3] E. Gottlieb,[3] B. C. Daube,[3] and D. M. Matross[3]

Received 27 September 2006; revised 25 February 2007; accepted 19 March 2007; published 12 July 2007.

[1] Knowledge of trace gas fluxes at the land surface is essential for understanding the impact of human activities on the composition and radiative balance of the atmosphere. An ability to derive fluxes at the regional scale (on the order of 10^2–10^4 km^2), at the scale of ecosystems and political borders, is crucial for policy and management responses. Lagrangian ("air mass-following") aircraft experiments have potential for providing direct estimates of regional-scale fluxes by measuring concentration changes in air parcels as they travel over the landscape. Successful Lagrangian experiments depend critically on forecasts of air parcel locations, rate of dispersion of air parcels, and proper assessment of forecast errors. We describe an operational tool to forecast air parcel locations and dispersion and to guide planning of flights for air mass-following experiments using aircraft. The tool consists of a particle dispersion model driven by mesoscale model forecasts from operational centers. The particle model simulates time-reversed motions of air parcels from specified locations, predicting the source regions which influence these locations. Forecast errors are incorporated into planning of Lagrangian experiments using statistics of wind errors derived by comparison with radiosonde data, as well as the model-to-model spread in forecast results. We illustrate the tool's application in a project designed to infer regional CO_2 fluxes—the CO_2 Budget and Rectification Airborne study, discuss errors in the forecasts, and outline future steps for further improvement of the tool.

Citation: Lin, J. C., C. Gerbig, S. C. Wofsy, V. Y. Chow, E. Gottlieb, B. C. Daube, and D. M. Matross (2007), "Designing Lagrangian experiments to measure regional-scale trace gas fluxes", *J. Geophys. Res.*, *112*, D13312, doi:10.1029/2006JD008077.

1. Introduction

[2] Fluxes of gaseous species between the land surface and the atmosphere strongly affect the environment. Radiatively active species such as CO_2, CH_4, and N_2O emitted from human activities are believed to have the potential to bring about climate change [*Intergovernmental Panel on Climate Change* (*IPCC*), 2001]. Emissions of NO_x and hydrocarbons alter the chemistry of the atmosphere and lead to production of tropospheric O_3 and adverse air quality [*Brasseur et al.*, 1999]. Evaporation controls the Earth's surface energy and hydrological balance, as well as the dynamics of the atmosphere [*Peixoto and Oort*, 1992].

[3] Directly measuring the surface sources and sinks for these gaseous species at the regional scale (10^2–10^4 km^2) has been challenging [*Brasseur et al.*, 1999; *Parlange et al.*, 1995; *Wofsy and Harriss*, 2002]. Complete ground-based sampling at the relevant scales is difficult due to resource limitations and logistical difficulties. Spaceborne sensors cover regional to global scales, but they are generally less sensitive to concentration changes in the planetary boundary layer (PBL) [*Liou*, 2002], where signals of surface fluxes are strongest.

[4] Estimates of regional source/sink distributions have often been derived from scaling up local measurements [*Ehleringer and Field*, 1993; *Parrish et al.*, 2002] rather than relying on direct observations. However, upscaling is often subject to large errors over a heterogeneous landscape. Independent estimates are needed to evaluate and test these upscaling methods.

[5] Lagrangian experiments repeatedly measure concentrations of target species in an ensemble of air parcels as they travel over the landscape [*Lin et al.*, 2004; *Lin et al.*, 2006]. Such experiments are uniquely suited to provide direct measurements of regional-scale fluxes that are difficult to derive from other means. Air parcels are transported across long distances (several hundred km) over 1 day, given a typical wind speed of ~10 m/s. Net changes in concentrations of gaseous species in air parcels as they travel across the landscape reveal the strength of sources/sinks along their transport path.

[6] While "Lagrangian experiments" may often be interpreted as "air mass following", atmospheric disper-

[1]Department of Earth and Environmental Sciences, University of Waterloo, Waterloo, Ontario, Canada.
[2]Max-Planck-Institut für Biogeochemie, Jena, Germany.
[3]Department of Earth & Planetary Sciences and Division of Engineering & Applied Sciences, Harvard University, Cambridge, Massachusetts, USA.

Copyright 2007 by the American Geophysical Union.
0148-0227/07/2006JD008077$09.00

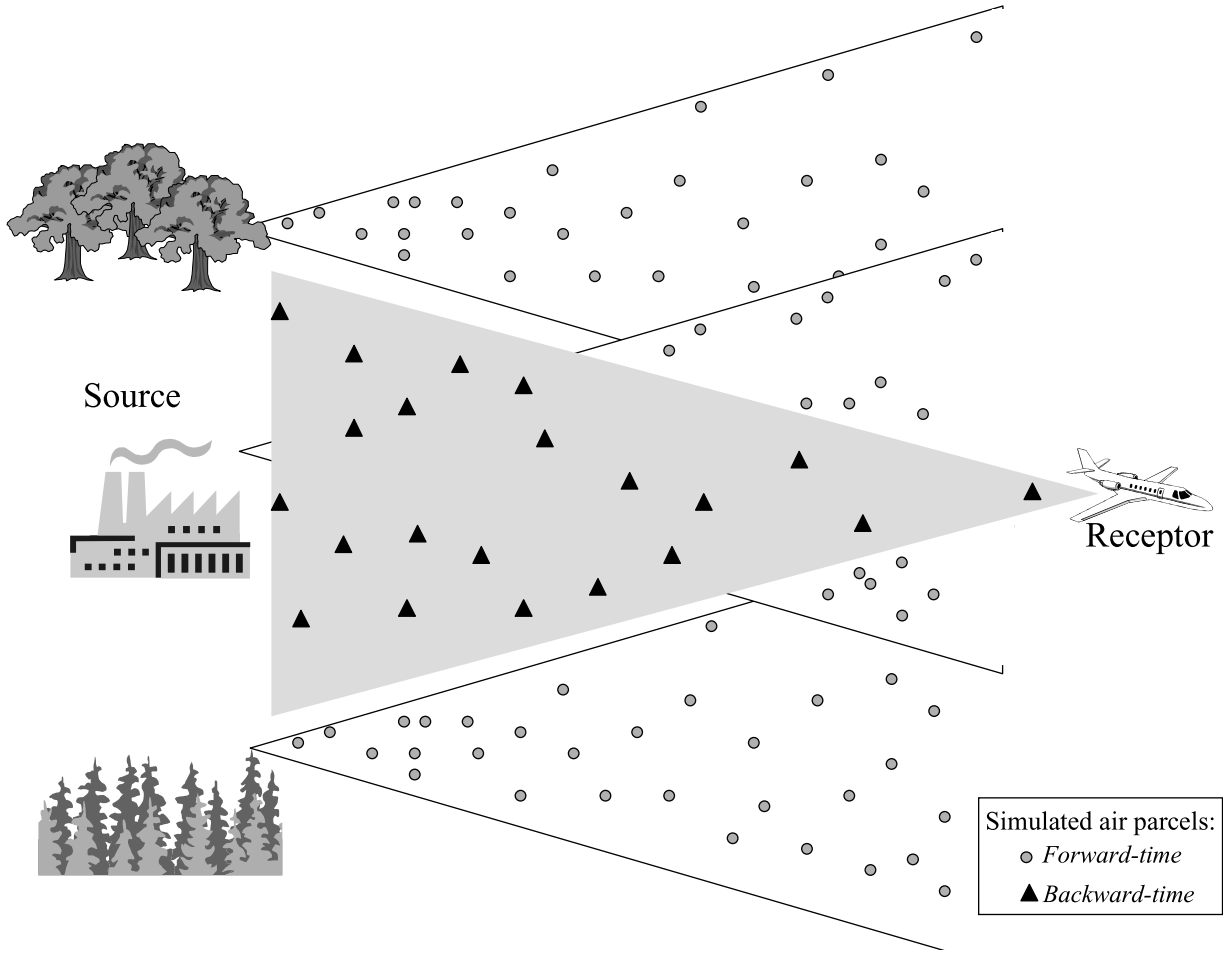

Figure 1. The relationship between backward- and forward-time transport of air parcels, represented by grey circles and black triangles, respectively. Dispersion causes air parcels arriving at a measurement location (receptor) to originate from numerous upwind source regions. Backward-time simulations from Lagrangian particle dispersion models, which model the effects from dispersion, elucidate the source regions with a single run.

sion causes air parcels originally found within a single air mass to be separated from one another (Figure 1). Air parcels separated by dispersion and advected by winds over hundreds of kilometers necessitate an airborne sampling platform. Aircrafts are especially suited for implementing Lagrangian experiments due to their capability to carry out three-dimensional sampling and cover the relevant distances.

[7] Implementing Lagrangian experiments requires a proper tool to forecast the locations of air parcels and their rate of dispersion in order to plan suitable flight patterns for the sampling program.

[8] In this paper we describe a tool that incorporates a particle dispersion model to design Lagrangian experiments for measuring regional-scale sources/sinks of gases. The tool places special emphasis on meeting the following criteria for an effective flight planning tool, described in detail in the next section: (1) simulation of dispersion, (2) computational efficiency, and (3) quantitative assessment of forecast errors.

[9] To our knowledge, only a single paper [*Stohl et al.*, 2004] has previously described a modeling system to aid in Lagrangian flight planning in the troposphere. These authors have likewise employed a particle dispersion model, combining it with Eulerian concentration fields to enable pollution plumes to be followed from North America to Europe with multiday Lagrangian experiments. Our paper differs from that of *Stohl et al.* [2004] in two important respects: First, we focus on estimating surface fluxes rather than tracking pollution plumes. Second, we introduce a new way to assess forecast errors by various means: incorporating stochastic wind errors, using multimodel ensembles, and determining the stability of forecasts derived from runs of the same model at different forecast times.

[10] We describe in this paper details of the forecasting tool (section 3), and we illustrate the use of the tool (section 4) in the CO_2 Budget and Rectification Airborne (COBRA) study [*Gerbig et al.*, 2003a], which sought to measure the regional release and uptake of CO_2 by the

terrestrial biosphere [*Lin et al.*, 2004]. We conclude with a discussion of future improvements and directions.

2. Requirements of Lagrangian Experiment Planning Tool

2.1. Simulation of Dispersion

[11] Lagrangian experiments require air parcels to be sampled repeatedly near sources/sinks, often in the lower troposphere and PBL where wind shear and turbulence are particularly pronounced [*Stull*, 1988], causing air parcels initially found close to one another to disperse significantly over time. Strong dispersion means that air parcels found at an observation location (''receptor'') arrive from numerous upwind locations (Figure 1), and this feature must be quantitatively simulated by the flight planning tool. Conventional back trajectory models fail to meet this requirement, as trajectories generated by interpolating mean winds cannot properly simulate dispersion [*Stohl*, 1998]. Accounting for dispersion is particularly important if upwind sources are distributed heterogeneously across the land surface. For example, CO_2 fluxes differ markedly between croplands, coniferous forests, urban areas, and grasslands [*Baldocchi et al.*, 2001]. Dispersion causes the receptor to be influenced by a source region distributed over an area, with differing fluxes, rather than a narrow source region lying along a single trajectory (Figure 1). Neglect of wind shear in flight planning, i.e., assuming an entire atmospheric column to be advected in a single direction, can severely limit instances when Lagrangian experiments can be conducted [*Lloyd et al.*, 2001; *Schmitgen et al.*, 2004].

2.2. Accounting for Forecast Uncertainties

[12] Forecasts inevitably contain uncertainties that cause forecasted air parcel trajectories to deviate from actual trajectories in the atmosphere [*Draxler*, 2003; *Straume et al.*, 1998]. Flights based on uncertain forecasts potentially sample air parcels that are not linked in a Lagrangian sense to the receptor. Thus the forecasting tool needs to incorporate these uncertainties in order to provide robust flight plans which reduce the sensitivity to such errors. This requirement is, like the dispersion requirement, made more stringent if sources/sinks are heterogeneous [*Gerbig et al.*, 2003a]. Heterogeneous sources/sinks give rise to upwind tracer gradients that, if not properly characterized, result in uncertainties in the sources/sinks inferred from Lagrangian experiments (see the papers of *Lin et al.* [2004] and *Lin et al.* [2006] for specific examples).

2.3. Computational Efficiency

[13] Computational efficiency enables numerous possibilities for the flight planning tool: use of rapid updates from numerical weather prediction (NWP) centers, ensemble simulations to probe sensitivity to model formulation, and flexibility to test out different ideas. NWP centers improve forecast quality by continuously assimilating observations to refine estimates for the state of the atmosphere [*Kalnay*, 2002; *Parrish et al.*, 1997; *Rabier et al.*, 2000]. In order to incorporate the refined forecasts from NWP centers, the flight planning tool needs to be computationally efficient, such that flight planning products can be rapidly updated as new forecasts are released (section 3.3.2). Computational efficiency also allows ensemble runs to be carried out, using different model products or the same model at different forecast times, while keeping up with the NWP updates [cf. *Kalnay et al.*, 1998; *Straume et al.*, 1998].

3. The Flight Planning Tool

[14] We present a flight planning tool that satisfies the requirements described in the previous section, based on the Stochastic Time-Inverted Lagrangian Transport (STILT) model [*Lin et al.*, 2003], a particle dispersion model. Particle models have specifically been developed to simulate turbulent dispersion [*Obukhov*, 1959; *Rodean*, 1996; *Smith*, 1968]. STILT is built upon a modified version of the Fortran source code from the NOAA Air Resources Laboratory (ARL) HYSPLIT model [*Draxler and Hess*, 1997; *Draxler and Hess*, 1998]. The flight planning tool includes UNIX shell scripts and programs written in the higher-level R language [*R Development Core Team*, 2004], which call STILT, process the particle output, and generate results in both tabular and graphical format. In this section, we first describe the STILT model (section 3.1) and then present a sample output from the tool (section 3.2). We then elaborate on the various ways in which the flight planning tool accounts for forecast errors (section 3.3).

3.1. STILT

[15] STILT meets the requirements outlined in section 2 in the following ways. STILT simulates turbulence with stochastic deviations from the mean wind and explicitly models the interaction between stochastic velocities and the mean wind shear, the basic cause for dispersion in the atmosphere. The particles (representing air parcels) start from the receptor and are transported backward in time, marking out the upwind source regions (Figure 1) and providing an especially efficient method to incorporate the effects of dispersion [*Stohl et al.*, 2003; *Uliasz and Pielke*, 1990]. The stochastic nature of STILT also means that ''error velocities'' can be added to the motion of the particles to incorporate forecast errors [*Lin and Gerbig*, 2005] (section 3.3.1). *Lin et al.* [2003] have shown that in a physically consistent model, a single backward-time simulation provides the same information as many more forward-time simulations from all potential upwind source regions and time steps. Thus the backward-time simulation provides a significant reduction in computational cost.

[16] STILT is an ''off-line'' model, driven with meteorological fields generated by other models that numerically integrate the dynamical equations of the atmosphere. The off-line character of STILT further translates into a low computational cost. A simulation using 1000 particles running for 24 hours backward in time typically takes 10 min on an Intel Xeon 2.4 GHz system with 512 K cache and 2 Gb of RAM running RedHat 9. This means that even with a single processor, numerous runs can be completed during the 6-hour update time between different NWP forecasts. The off-line characteristic provides the flexibility to use different meteorological fields as well, enabling the construction of multimodel ensembles to assess model errors (section 3.3).

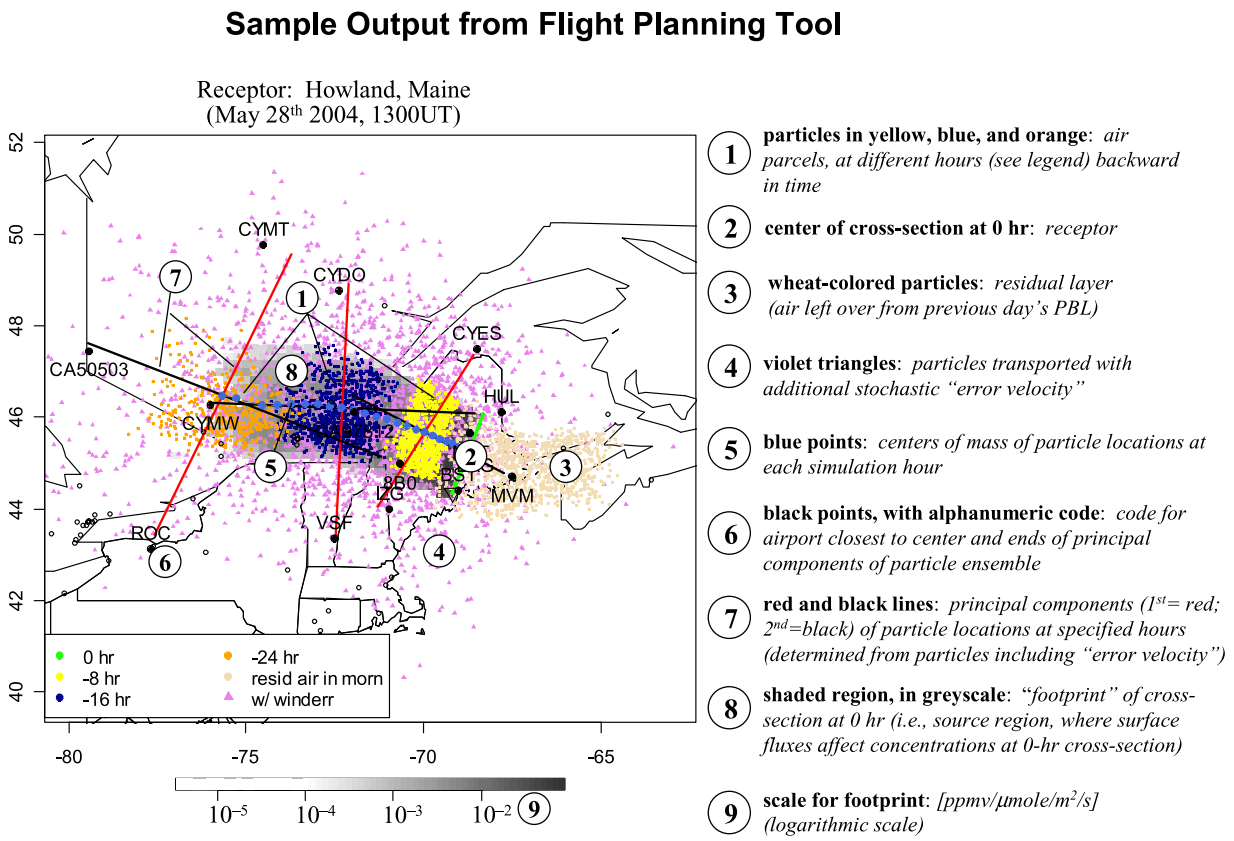

Figure 2. An example of the graphical product generated by the flight planning tool. The receptor is Howland, Maine, which is the center of the downwind (0 hour) cross section from where particles are simulated backward in time in STILT. The release time is on 28 May, 1300 UT, and in this example, the STILT particles are driven with meteorological fields from the AVN model updated on 25 May, 0600 UT. The different components of the figure are tagged with numbers that are linked to explanations on the side.

[17] Currently, STILT is driven with meteorological fields, updated every 6 hours, from the following operational forecast models: AVN (191 km) [*Kanamitsu et al.*, 1991], ETA (12 + 40 km) [*Black*, 1994], and MM5 (15 + 45 km) [*Grell et al.*, 1994]. The MM5 simulations are conducted by the U.S. Air Force; the other products are generated by the National Centers for Environmental Prediction (NCEP). We downloaded these fields from NOAA ARL [*Rolph*, 2003]. Recently, the capability to drive STILT with RAMS [*Cotton et al.*, 2001], ECMWF [*Palmer et al.*, 2000], and WRF [*Michalakes et al.*, 2001] fields has also been implemented.

3.2. Sample Output

[18] Figure 2 shows an example of a STILT simulation generated by the forecasting tool, with the receptor placed at the Howland eddy flux tower in central Maine [*Hollinger et al.*, 1999]. The Howland tower is placed at the center of a line, oriented along the cross-wind direction (shown in green), where particles were released into STILT on 28 May 2004, at 1300 UT, and transported backward in time. The particles are shown at −8 (yellow), −16 (blue), and −24 hours (orange) from the time of release, marking the upwind source regions where air parcels are found. The particles spread over wider regions as they travel backward in time, reflecting the dispersive effects of turbulence and wind shear in the model. The violet particles indicate air parcel trajectories that incorporate forecast errors in the form of stochastic velocities (see section 3.3.1).

[19] The shaded regions represent the "footprint," the areas where surface fluxes contribute to changes to concentrations at the receptor. The footprint is in units of [ppmv/(μmol/m^2/s)], indicating the sensitivity of receptor concentrations (ppmv) to surface fluxes (μmol/m^2/s), and is calculated by integrating the amount of time that particles are found within the PBL (see *Gerbig et al.* [2003b] and *Lin et al.* [2003] for details). In Figure 2, the shaded regions indicate the 24-hour integrated footprint, so differences in tracer concentrations between the receptor observations (green) and those measured 24 hours earlier (orange) reflect the net contribution of surface fluxes within the footprint region. Thus the footprint region is the area where atmospheric measurements have "leverage" in constraining surface fluxes.

[20] The center of mass of the ensemble of particles at each hour is shown in Figure 2 as a blue point. In addition, as indicators of particle spread and orientation, the first and second principal components (eigenvectors associated with the two largest eigenvalues) of the particle locations are plotted for −8, −16, and −24 hours as the red and black

lines, respectively. These lines show the dominant orientations of the particle ensemble, and their lengths encompass 90% of the particles along the principal components. We used the violet-colored particles at each hour to determine the principal components in order to include the effect of forecast errors, which resulted in a wider spread of particles and a lengthening of the principal components, reflecting uncertainties in the air parcel locations (section 3.3.1).

[21] The tool includes an airport database and automatically determines the airports that are closest to the ends and centers of the particle ensemble. The selected airports are shown for the specified hours as black points, along with their airport codes. Airports with "instrument approach systems" provide locations where vertical sampling can be conducted to the ground surface even during cloudy conditions, enabling representative sampling of concentrations in the PBL. The significance of such airports will be discussed in more detail in section 4.1.

[22] The wheat-colored particles denote air parcels in the residual (or "relic") layer [*Stull*, 1988], which were found within the same PBL during the previous afternoon as air parcels arriving at the receptor but are found above the shallow PBL over the receptor in the morning. It is particularly interesting to identify residual-layer air for comparison to early-morning observations near the ground at the receptor. Air in the residual layer becomes decoupled from surface fluxes after PBL mixing ceases at night, and hence concentrations in the residual layer are unchanged by nocturnal surface fluxes. By identifying and sampling air in the residual layer (generally found downwind of the receptor due to higher wind speeds than those within the shallow nighttime PBL), concentrations in the PBL from the previous afternoon can be inferred even if they were not directly observed. Thus the difference between concentrations in the residual layer and in the morning PBL at the receptor provides an estimate of changes that occurred over the nighttime (see section 4.2).

3.3. Accounting for Forecast and Model Errors

[23] The flight planning tool includes several independent methods to quantify and assess the impact of errors on the forecast results. We describe each of them below.

3.3.1. Incorporate Forecast Error Statistics in Particle Motion

[24] STILT has the capability to incorporate uncertainties in wind vectors as an additional stochastic "error velocity" that transports each particle [*Lin and Gerbig*, 2005]. Particles transported with these additional stochastic motions are generally dispersed over a larger spatial area, reflecting the additional uncertainty about air parcel locations due to errors in the forecasted wind fields.

[25] The statistics of the error velocity were estimated from directly comparing forecasted winds and radiosonde observations over the coterminous U.S. from the NOAA Forecast Systems Laboratory database [*Schwartz and Govett*, 1992] and the ARM/CART program [*Stokes and Schwartz*, 1994]. Figure 3 shows the RMS error in the U component of the wind as a function of the number of hours extending into the future for the different forecasted fields during May and June 2003. For all the models, the RMS error increases as the forecast extends further into the future. We are currently unclear as to why the higher-resolution

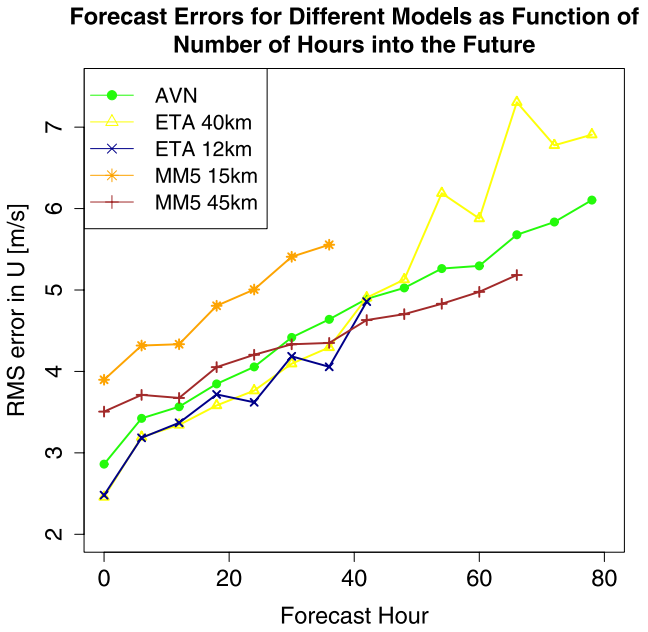

Figure 3. RMS errors in the U component (west to east) of horizontal wind, derived from direct comparison with radiosonde observations below 10-km ASL in the U.S. during May–June 2003. Winds from different forecast models are linearly interpolated to the locations of the radiosondes for the comparison. The errors are shown as a function of the number of hours the forecasts extend into the future. These error statistics are used to parameterize an additional "error velocity" in the STILT simulations in order to incorporate forecast errors into flight planning (see violet particles in, for example, Figure 2).

15-km version of MM5 exhibited larger errors than the 45-km version.

[26] We assume a Gaussian distribution of errors at the current time with standard deviations from Figure 3, and prescribe these error velocities in horizontal directions by assuming serial correlation of 4 hours, spatial correlations with vertical length scale (decorrelation scale) of 900 m, and horizontal length scale of 120 km. These correlation values were originally determined [*Lin and Gerbig*, 2005] by comparing radiosonde observations with analyzed (instead of forecasted) winds from the Eta Data Assimilation System [*Black*, 1994].

[27] The violet triangles in Figure 2 are particles simulated with the additional error wind velocities in the horizontal directions at the specified hours: 0, −8, −16, and −24. The violet triangles mark out a wider region than those without the error velocity during all hours. By planning flights that sample over the wider region, we expect to be able to sample the upwind air parcels which would arrive at the receptor even in the presence of forecast errors.

3.3.2. Multimodel Ensemble

[28] Comparisons between simulations from different atmospheric models have commonly been used to probe the sensitivity of results to different numerical schemes and parameterizations [*Denning et al.*, 1999; *IPCC*, 2001].

[29] The forecasting tool has the capability to conduct ensemble simulations using the different forecast models

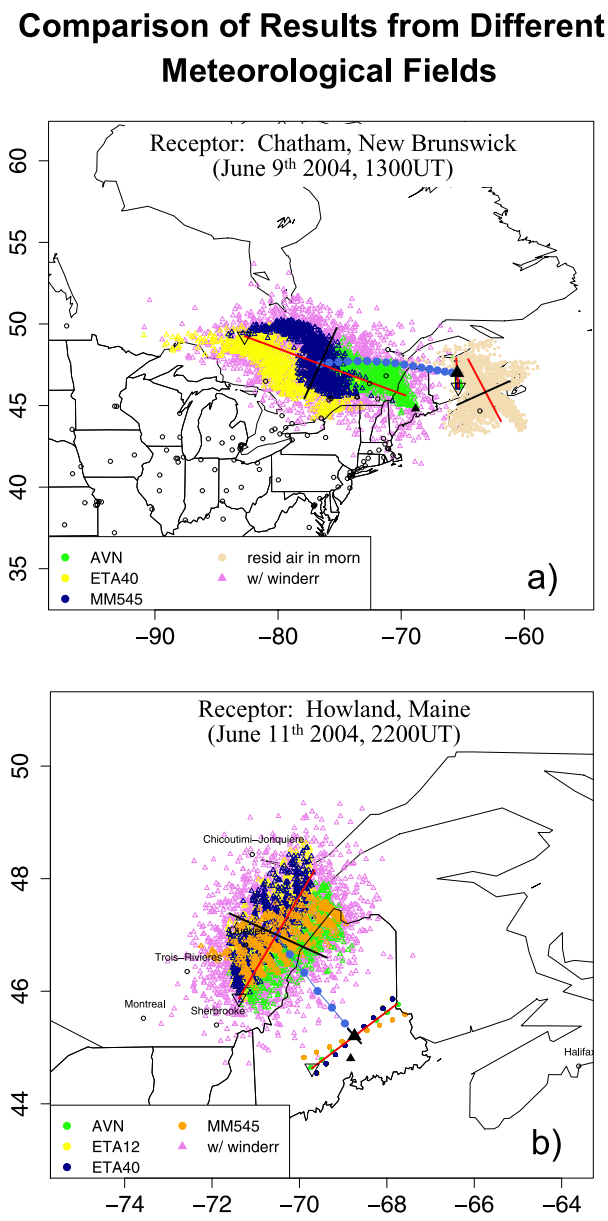

Figure 4. A comparison of STILT simulations using forecast meteorological fields generated by different models for two instances: (a) receptor located at Chatham, New Brunswick, on 9 June, 1300 UT (based on forecasts on 7 June, 1200 UT), and particles shown at −16 hours; (b) receptor located at Howland, Maine, on 11 June, 2200 UT (based on forecasts on 10 June, 0600 UT), and particles shown at −6 hours. Note that, unlike Figure 2, the different-colored particles do not represent different hours, but the results for the same hour generated using different meteorological files.

(AVN, ETA, and MM5) and then to overlay the simulated STILT particle locations on the same plot to reveal the degree to which forecasts are model-dependent. Discrepancies between models are then interpreted as an indication of forecast errors.

[30] For instance, STILT simulations driven with the AVN, ETA (40 km), and MM5 (45 km) are overlaid in Figure 4a for a receptor located at Chatham, New Brunswick, on 9 June 2004. Note that the various-colored particles in Figure 4 refer to different atmospheric models at the same hour rather than different times, as was the case for Figure 2. The particle locations at −16 hours differed significantly, with the ETA particles being found in Ontario, whereas the AVN and MM5 particles were dispersed over different parts of southern Quebec. The results diverged drastically in this example because the propagation of the warm front that moved through the region on 8 June differed greatly between the models. The model comparison alerted the flight planners to the significant uncertainty existing in the forecasted position of the warm front, and we decided not to conduct an experiment this day.

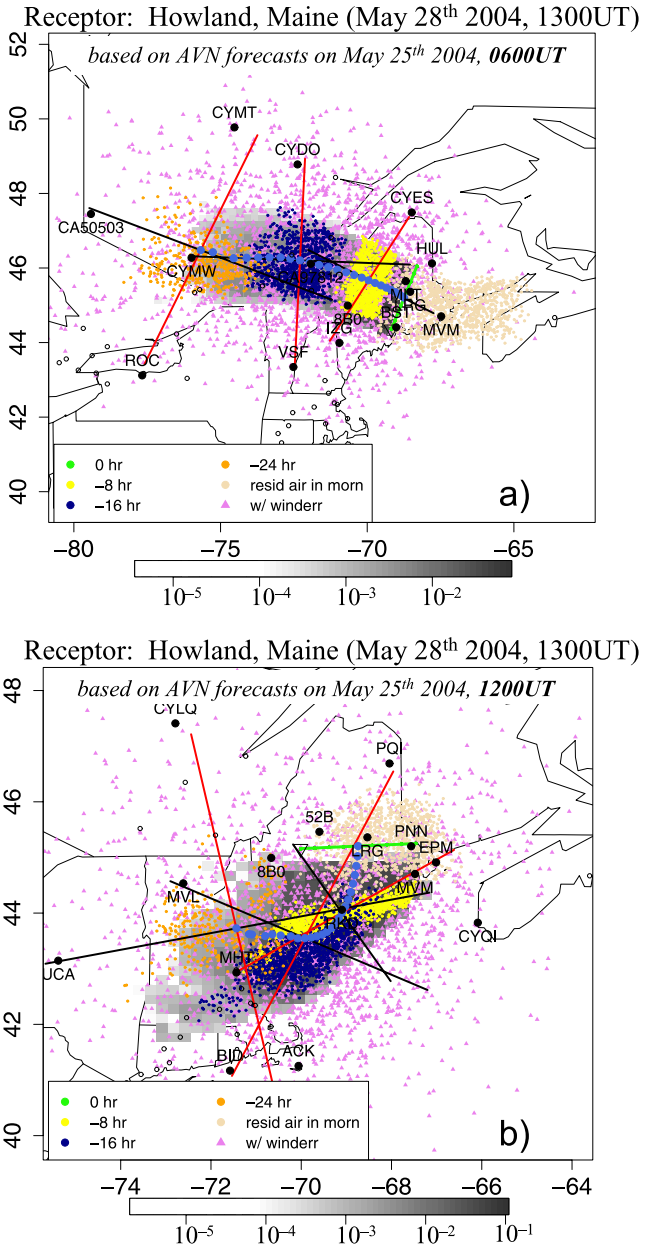

Figure 5. Outputs that are similar to Figure 2 but driven with AVN fields updated on (a) 25 May, 0600 UT, and (b) 25 May, 1200 UT.

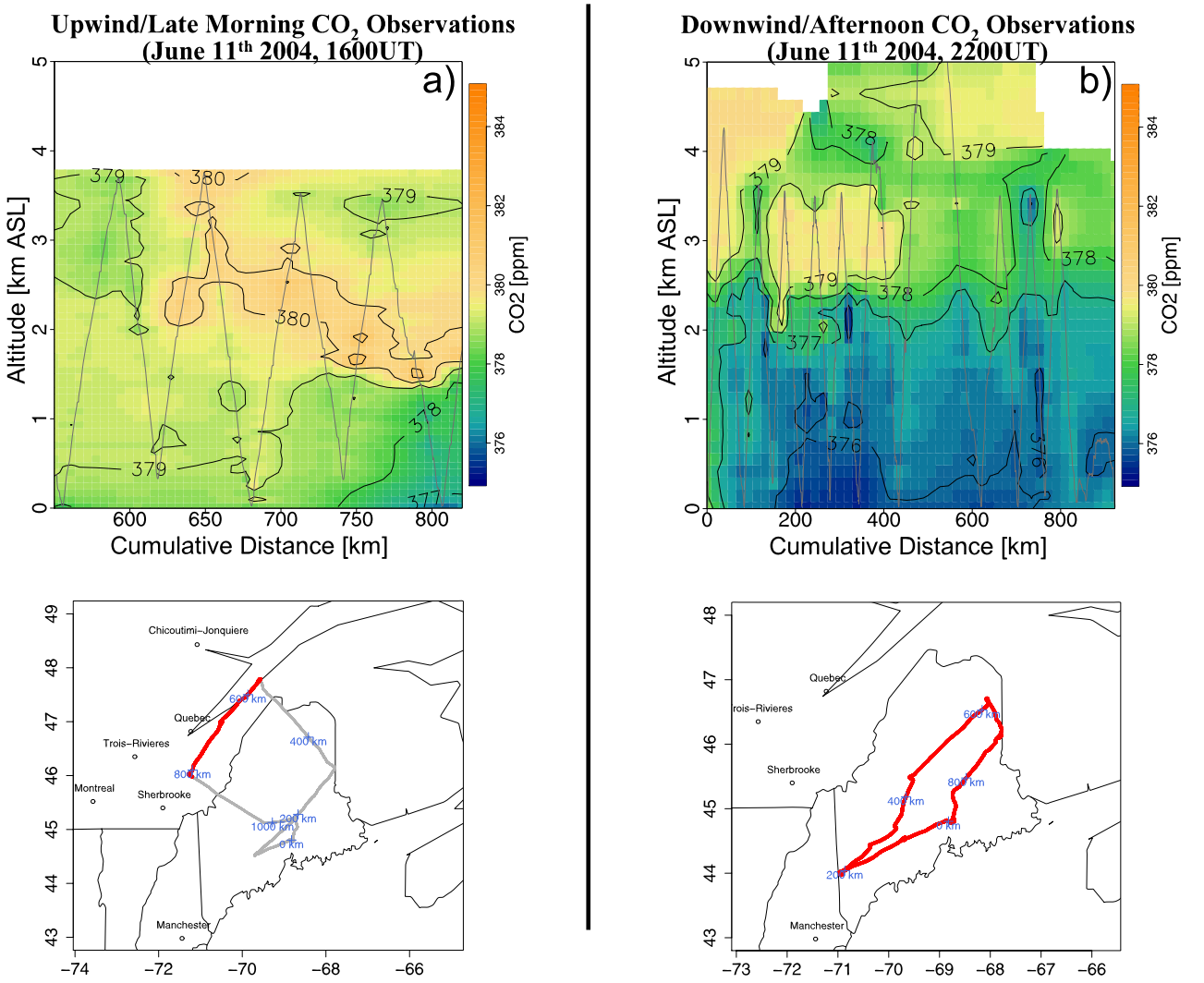

Figure 6. Observations and flight tracks from the (a) morning and (b) afternoon of 11 June. The CO_2 observations are shown as altitude-versus-cumulative-distance cross sections. The gray lines in the cross sections are the flight tracks, where direct observations were made; the cross section was constructed by a kriging method. The flight tracks are shown on maps in the lower panel; the lines in red are the subset of the flight used to create the cross section. The blue crosses label the cumulative distances during each flight.

[31] In contrast, the simulations by different models agreed closely for a receptor located at Howland, Maine, on 11 June 2004 (Figure 4b). All four models predicted particles at 6 hours backward in time to cover the Saint Lawrence River in Quebec. The different models converged in this case probably because there was no strong synoptic activity, and winds were under the influence of a large-scale high-pressure system covering the entire New England, Quebec, and Ontario regions. We carried out this Lagrangian experiment (for details, see section 4.1).

3.3.3. Stability of Particle Trajectories Over Different Forecasts

[32] The stability of forecasts generated by the same atmospheric model using different updates provided a further probe of forecast errors. We interpreted notable lack of stability in the forecasts to indicate instances in which forecasts were uncertain. For example, the simulation for the Howland receptor on 28 May, 1300 UT (Figure 5), changed drastically in 6 hours between the forecasts updated on 25 May, 0600 UT, and later at 1200 UT. This is especially obvious in the change of the trajectory for the center of mass of the particle ensembles (blue points in Figure 5). The forecasted locations further changed during the following day (not shown).

4. Examples of Flight Planning During the COBRA 2004 Experiment

[33] We illustrate in this section how the flight planning tool was used to design Lagrangian experiments during the CO_2 Budget and Rectification Airborne study (COBRA) mission in 2004. The goal of COBRA was to quantify regional fluxes of CO_2 by combining dedicated observations and models [*Gerbig et al.*, 2003b; *Lin et al.*, 2004]. The 2004 mission focused especially on constraining fluxes

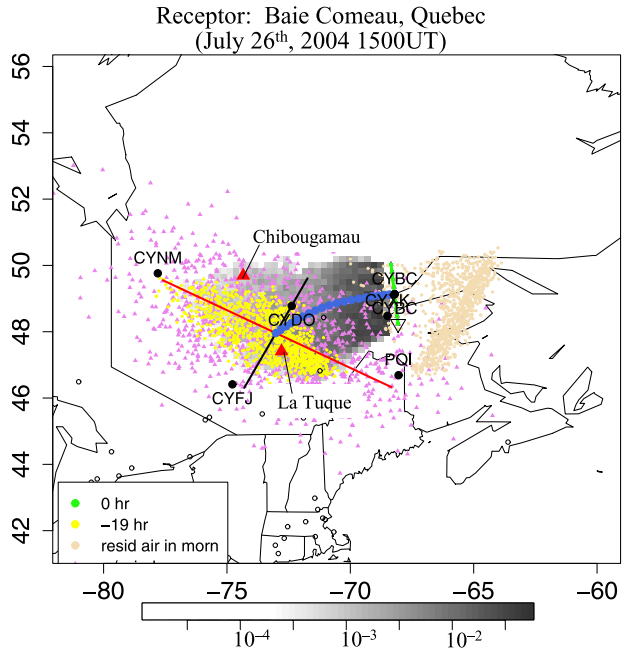

Figure 7. Output from the flight planning tool for the receptor in Baie Comeau, Quebec, on 26 July at 1500 UT. The result was based upon AVN forecasts updated on 24 July at 1200 UT. This output was used to plan flights to sample air parcels on the afternoon of 25 July (−19 hours) and at the receptor, thus bracketing the nighttime period dominated by respiration. The flight tracks and observations from this experiment are shown in Figure 8.

in the northeastern part of North America (specifically, New England + southern Quebec) from May through August.

[34] The COBRA aircraft was the University of Wyoming King Air [http://flights.uwyo.edu/] equipped for in situ measurements of CO [*Gerbig et al.*, 1999] and CO_2 [*Daube et al.*, 2002].

[35] CO_2 exhibits the following two special characteristics that need to be considered in flight planning: (1) Surface fluxes of CO_2 are distributed throughout the landscape [*Ehleringer and Field*, 1993], unlike emissions of pollutant species, most of which are located in urban centers. Accurate flight planning is therefore necessary to account for dispersion and forecast errors to properly determine upwind air parcel locations (sections 2.1 and 2.2). Failure to properly model upstream parcel locations means that observed changes in CO_2 can be attributed to erroneous subregions of the spatially distributed CO_2 fluxes. Furthermore, if upwind locations are falsely forecasted, but are properly simulated in the analysis, the failure to measure the upwind air mass can cause large errors in fluxes inferred from the Lagrangian experiments [*Lin et al.*, 2004; *Lin et al.*, 2006]. (2) Strong diurnal contrast between nighttime emissions of CO_2 from respiration and daytime uptake from photosynthesis [*Goulden et al.*, 1996; *Wofsy et al.*, 1993]. The diurnal sign reversal in CO_2 fluxes calls for observations to separately characterize nighttime release and daytime uptake of CO_2.

[36] Here we present two examples from COBRA, one designed to constrain daytime photosynthetic fluxes and the other to constrain nighttime release from respiration.

4.1. Daytime Constraint

[37] We planned flights to sample the air at −6 (morning, upwind) and 0 hours (afternoon) at the receptor at Howland, Maine, on 11 June, 2200 UT. The results from the forecasting tool (in the form of multimodel comparisons) are shown in Figure 4b. The change in CO_2 concentrations between those two times reflects the effect of daytime fluxes, dominated by photosynthetic uptake. To sample the air parcels 6 hours before arriving at Howland (Figure 6a), the aircraft conducted profiles into airports including Riviere du Loup, along the St. Lawrence River, and Montmagny to the southwest. Each profile into an airport was a "missed approach," a standard aeronautical maneuver in which the aircraft follows published procedures and profiles into an airport as if conducting a landing. The aircraft descended at these rural airports to altitudes as low as several meters above the runway and then climbed out of the airport. The missed approaches into airports enabled the aircraft to descend to altitudes well within the shallow morning PBL even under cloudy conditions, when limited visibility would otherwise restrict opportunities for low-altitude sampling in airspace away from airports. The forecasting tool automatically displays airports closest to the center of mass of the particle ensemble and the ends of the two principal components of the ensemble (Figure 2), facilitating the choice of such airports.

[38] The CO_2 concentrations from this experiment are shown in Figure 6 as altitude-versus-cumulative-distance cross sections, with flight tracks displayed as gray lines. A marked difference is observed in the lower troposphere, where CO_2 concentrations were notably lower in the afternoon over the receptor by ~3 ppmv. The change in concentration over 6 hours provides a direct measure of daytime uptake of CO_2 by the vegetation [cf. *Lin et al.*, 2004].

[39] A detailed description of how observations from such Lagrangian experiments are used to constrain regional-scale CO_2 fluxes can be found in the study of *Lin et al.* [2004]. In brief, the analysis proceeds as follows: the upwind observations are linked to the downwind observations with STILT-simulated air parcels, driven with assimilated (rather than forecasted) wind fields. Differences (downwind − upstream) in CO_2 column amounts are then divided by the elapsed time to produce observed fluxes. These fluxes reflect sources/sinks throughout the regional-scale footprint source region and can be compared against predictions from a biospheric model, which attempts to incorporate the spatiotemporal heterogeneity arising from biological factors as well as environmental drivers (for example, radiation and temperature). Discrepancies between observed fluxes and modeled fluxes are then minimized by adjusting parameters in the biospheric model, for example, within the framework of a formal Bayesian inversion.

4.2. Nighttime Constraint

[40] An example of Lagrangian observations to constrain nighttime CO_2 emissions was based on the output from the planning tool shown in Figure 7. For this experiment, the receptor was located in Baie Comeau, Quebec, in the morning at 1500 UT on 26 July. Sampling was conducted at the receptor and 19 hours upwind (afternoon of previous day), bracketing the nighttime, to measure the net change in CO_2 concentrations arising from net respiration in the region. The −19-hour air parcels were

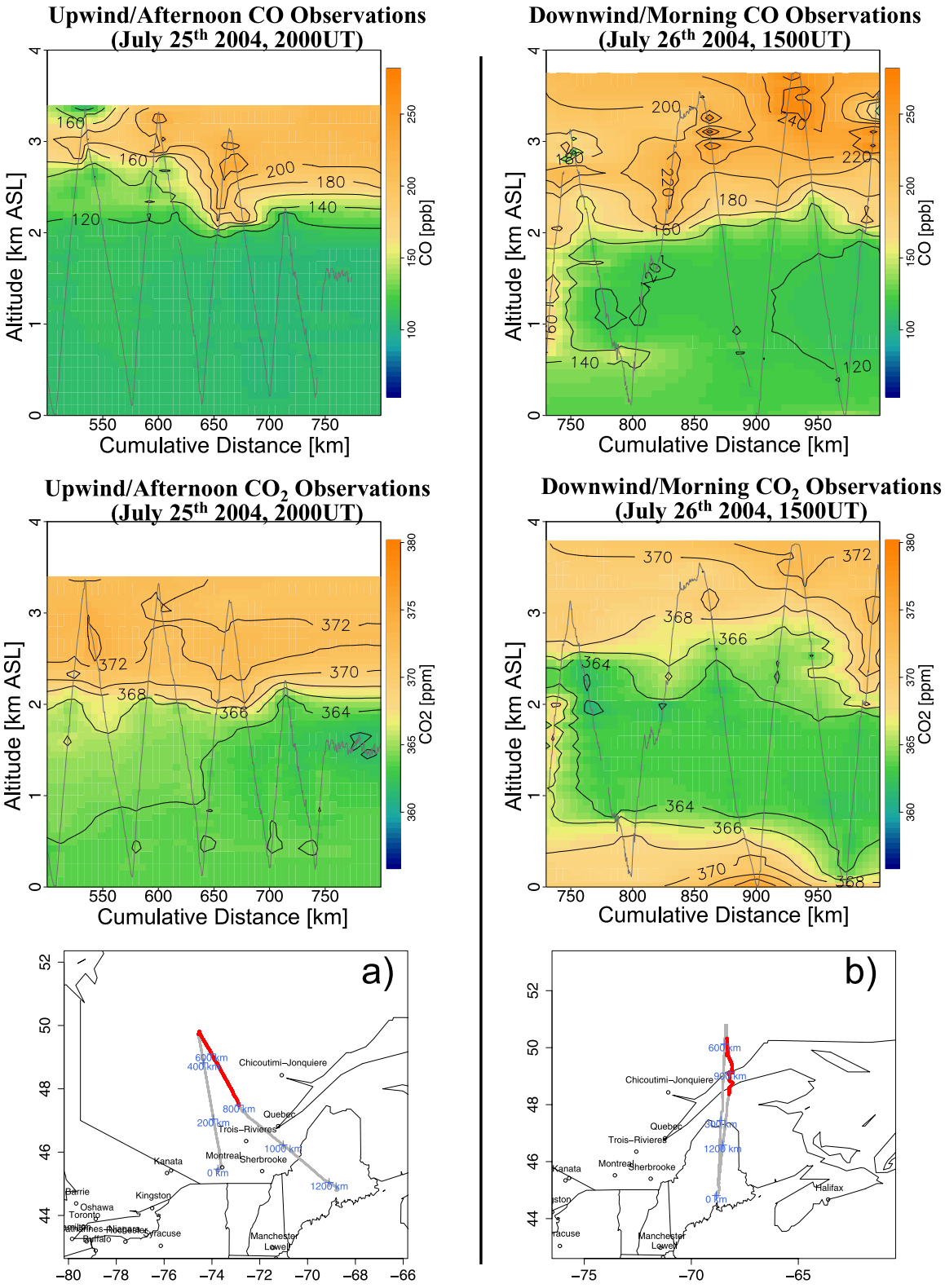

Figure 8. Similar to Figure 6 but for the (a) afternoon of 25 July and (b) morning of 26 July. Both the observed CO and CO_2 cross sections are shown.

predicted to be over southern Quebec. In order to sample these parcels, the aircraft conducted missed approaches into and profiles between the airports of Chibougamau and La Tuque (shown as red triangles). These profiles only partially sampled the −19-hour parcels due to restrictions in flight duration. Likewise, the limited flight duration precluded direct sampling of residual-layer air parcels (wheat-colored) eastward of Baie Comeau during the morning of 26 July.

[41] The flexibility in receptor choice, made possible by the planning tool's computational efficiency, was critical for this experiment. We originally intended to place the receptor at Chibougamau. However, the westerly wind caused air parcels upwind of Chibougamau to be situated far west in Ontario. The footprint (shaded area) in this case would then not have been situated within the COBRA study area of southern Quebec. We thus moved the receptor further east, to Baie Comeau, in order to shift the footprint eastward from Ontario to Quebec.

[42] The observed CO_2 concentrations from this experiment (Figure 8) show enhancements in the range of 4–5 ppmv between the previous afternoon and the morning of 26 July in the altitudes below 1 km ASL within the shallow morning PBL. During both times, a plume of high CO was observed above 2 km ASL, probably due to the influence of large forest fires to the west of the study area. The interception of this CO plume in both cross sections lends support to the analysis indicating that the Lagrangian experiment was generally successful in resampling air parcels after 19 hours of travel.

[43] In the morning observations (Figure 8b), CO_2 concentrations ($\sim$364 ppmv) between 1- and 2-km ASL are lower by several parts per million by volume than values above 2 km or below 1 km. The air in this layer has yet to be affected by enhancements in the lowest altitudes and presumably is the residual layer, reflecting concentrations established in the PBL from the previous afternoon. The concentration of $\sim$364 ppmv is almost identical to the observed upwind PBL concentrations (Figure 8a) during the previous afternoon. Although parcels within the observed PBL at -19 hours, which end up in the residual layer, should be transported further eastward to locations marked out by the wheat-colored particles in Figure 7, which were not directly sampled, this comparison nonetheless is highly suggestive that concentrations in the residual layer may be similar to those from the previous afternoon's PBL. This would mean that sampling the residual layer during the morning provides an indirect way to infer concentrations from the previous afternoon, and differences between enhanced concentrations in the shallow morning PBL and lower concentrations in the residual layer provide a direct constraint on fluxes from nighttime respiration.

5. Summary and Conclusions

[44] Lagrangian experiments play an important role for producing direct observations of the sources/sinks of different atmospheric species over scales inaccessible by other means. Lagrangian experiments have wide applicability, providing a unique data set which serves to test and constrain models in such diverse disciplines as, for example, carbon science [*Wofsy and Harriss*, 2002], pollution research [http://www.al.noaa.gov/ICARTT/] [*Stohl et al.*, 2004], and aerosol studies [*Bates et al.*, 1998]. Furthermore, the direct measurements of fluxes from Lagrangian experiments can be used to complement surface-based long-term observational sites by verifying estimates derived solely from such observations [*Lin et al.*, 2006].

[45] We have described a tool to plan Lagrangian experiments based on a particle dispersion model that satisfies the following criteria: computational efficiency, dispersion capability, and the ability to account for forecast uncertainties. Particle-based dispersion models have originally been developed to specifically simulate turbulent dispersion. The backward-time nature of STILT, serving as the core of the planning tool, means that locations of air parcels arriving at an observation location can be estimated from a single model run [*Lin et al.*, 2003]. The stochastic nature of STILT also means that an additional "error velocity" [*Lin and Gerbig*, 2005] can be added to the motion of the particles to incorporate forecast errors. We further illustrated how the tool was used in the 2004 COBRA mission to constrain regional-scale carbon fluxes. This paper, like the one of *Stohl et al.* [2004], demonstrates the potential of tools based on particle dispersion models to aid in carrying out Lagrangian experiments.

[46] We have focused exclusively on applying the tool in the backward-time mode to elucidate the upwind influence at a measurement location. However, in the case of field experiments seeking to track specific plumes (for example, from forest fires or urban areas), the tool can be similarly applied by simulating particle transport forward in time.

[47] Future improvements to the STILT-based planning tool will include the capability of incorporating uncertainties in not just the horizontal velocities but also errors in vertical redistribution [*Gerbig et al.*, 2006; *Lin et al.*, 2006] from processes such as convection and turbulent mixing within the PBL. Such processes are critical for tracer transport [*Thompson et al.*, 1994] and inference of surface fluxes [*Law et al.*, 1996] but remain difficult to reproduce in STILT due to limitations in the meteorological input as well as model parameterizations [*Gerbig et al.*, 2003b; *Gerbig et al.*, 2006]. Additionally, real-time assimilation of meteorological observations from the research aircraft by the flight planning tool can be used to reveal errors in the original forecasts and to realize improvements in the transport of air parcels.

[48] **Acknowledgments.** We thank the University of Wyoming King Air aircraft team for their dedication, expertise, and humor in enabling the successful coordination between flight planning and execution during COBRA 2004. We appreciate the invaluable help in computing from Aaron Culich at Harvard and the operational weather forecasts from Meridian Environmental Technology. We also gratefully acknowledge the NOAA ARL for the provision of the forecast meteorological fields used in this publication. The 2004 COBRA flights were supported by the National Science Foundation's Biocomplexity in the Environment program (ATM-0221850).

References

Baldocchi, D., et al. (2001), FLUXNET: A new tool to study the temporal and spatial variability of ecosystem-scale carbon dioxide, water vapor and energy flux densities, *Bull. Am. Meteorol. Soc.*, *82*, 2415–2435.

Bates, T. S., B. J. Huebert, J. L. Gras, F. B. Griffiths, and P. A. Durkee (1998), International Global Atmospheric Chemistry (IGAC) project's First Aerosol Characterization Experiment (ACE 1): Overview, *J. Geophys. Res.*, *103*(D13), 16,297–16,318.

Black, T. L. (1994), The new NMC mesoscale Eta-model—Description and forecast examples, *Weather Forecast.*, *9*(2), 265–278.

Brasseur, G. P., J. J. Orlando, and G. S. Tyndall (1999), *Atmospheric Chemistry and Global Change*, 654 pp., Oxford Univ. Press, New York.

Cotton, W. R., et al. (2001), RAMS 2001: Current status and future directions, *Meteorol. Atmos. Phys.*, *82*, 5–29.

Daube, B. C., K. A. Boering, A. E. Andrews, and S. C. Wofsy (2002), A high-precision fast-response airborne CO2 analyzer for in situ sampling from the surface to the middle stratosphere, *J. Atmos. Oceanic Technol.*, *19*, 1532–1543.

Denning, A. S., et al. (1999), Three-dimensional transport and concentration of SF_6: A model intercomparison study (TransCom 2), *Tellus*, *51B*, 266–297.

Draxler, R. R. (2003), Evaluation of an ensemble dispersion calculation, *J. Appl. Meteorol.*, *42*, 308–317.

Draxler, R. R., and G. D. Hess (1997), Description of the HYSPLIT_4 modeling system, *NOAA Tech. Memo. ERL ARL-224*, 24 pp.

Draxler, R. R., and G. D. Hess (1998), An overview of the HYSPLIT_4 modelling system for trajectories, dispersion, and deposition, *Aust. Meteorol. Mag.*, *47*, 295–308.

Ehleringer, J. R., and C. B. Field (1993), Scaling physiological processes: Leaf to globe, 179-190 pp., Elsevier, New York.

Gerbig, C., S. Schmitgen, D. Kley, A. Volz-Thomas, K. Dewey, and D. Haaks (1999), An improved fast-response vacuum-UV resonance flourescence CO instrument, *J. Geophys. Res.*, *104*(D1), 1699–1704.

Gerbig, C., J. C. Lin, S. C. Wofsy, B. C. Daube, A. E. Andrews, B. B. Stephens, P. S. Bakwin, and C. A. Grainger (2003a), Toward constraining regional-scale fluxes of CO2 with atmospheric observations over a continent: 1. Observed spatial variability from airborne platforms, *J. Geophys. Res.*, *108*(D24), 4756, doi:10.1029/2002JD003018.

Gerbig, C., J. C. Lin, S. C. Wofsy, B. C. Daube, A. E. Andrews, B. B. Stephens, P. S. Bakwin, and C. A. Grainger (2003b), Toward constraining regional-scale fluxes of CO2 with atmospheric observations over a continent: 2. Analysis of COBRA data using a receptor-oriented framework, *J. Geophys. Res.*, *108*(D24), 4757, doi:10.1029/2003JD003770.

Gerbig, C., S. Korner, and J. Noilhan (2006), Uncertainties in atmospheric tracer modeling: Is there hope for quantification of regional scale greenhouse gas exchange fluxes through inversions?, in *European Geosciences Union Meeting*, Vienna, Austria.

Goulden, M. L., J. W. Munger, S.-M. Fan, B. C. Daube, and S. C. Wofsy (1996), Exchange of carbon dioxide by a deciduous forest: Response to interannual climate variability, *Science*, *271*, 1576–1578.

Grell, G. A., J. Dudhia, and D. R. Stauffer (1994), A description of the Fifth-generation Penn State/NCAR Mesoscale Model (MM5)., pp. 122, *NCAR Tech. Note TN-398 + STR*, Nat. Cent. for Atmos. Res., Boulder, Colo.

Hollinger, D. Y., S. M. Goltz, E. A. Davidson, J. T. Lee, K. Tu, and H. T. Valentine (1999), Seasonal patterns and environmental control of carbon dioxide and water vapor exchange in an ecotonal boreal forest, *Glob. Chang. Biol.*, *5*, 891–902.

Intergovernmental Panel on Climate Change (IPCC) (2001), *Climate Change: The Scientific Basis*, 944 pp., Cambridge Univ. Press, New York.

Kalnay, E. (2002), *Atmospheric Modeling, Data Assimilation, and Predictability*, 364 pp., Cambridge Univ. Press, New York.

Kalnay, E., S. J. Lord, and R. D. McPherson (1998), Maturity of operational numerical weather prediction: Medium range, *Bull. Am. Meteorol. Soc.*, *79*(12), 2753–2769.

Kanamitsu, M. (1991), Recent changes implemented into the Global Forecast System at NMC, *Weather Forecast.*, *6*(3), 425–435.

Law, R. M., et al. (1996), Variations in modeled atmospheric transport of carbon dioxide and the consequences for CO2 inversions, *Glob. Biogeochem. Cycles*, *10*(4), 783–796.

Lin, J. C., and C. Gerbig (2005), Accounting for the effect of transport errors on tracer inversions, *Geophys. Res. Lett.*, *32*, L01802, doi:10.1029/2004GL021127.

Lin, J. C., C. Gerbig, S. C. Wofsy, A. E. Andrews, B. C. Daube, K. J. Davis, and C. A. Grainger (2003), A near-field tool for simulating the upstream influence of atmospheric observations: the Stochastic Time-Inverted Lagrangian Transport (STILT) model, *J. Geophys. Res.*, *108*(D16), 4493, doi:10.1029/2002JD003161.

Lin, J. C., C. Gerbig, S. C. Wofsy, A. E. Andrews, B. C. Daube, C. A. Grainger, B. B. Stephens, P. S. Bakwin, and D. Y. Hollinger (2004), Measuring fluxes of trace gases at regional scales by Lagrangian observations: Application to the CO2 Budget and Rectification Airborne (COBRA) study, *J. Geophys. Res.*, *109*, D15304, doi:10.1029/2004JD004754.

Lin, J. C., C. Gerbig, S. C. Wofsy, B. C. Daube, D. M. Matross, V. Y. Chow, E. Gottlieb, A. E. Andrews, M. Pathmathevan, and J. W. Munger (2006), What have we learned from intensive atmospheric sampling field programs of CO2?, *Tellus*, doi:10.1111/j.1600-0889.2006.00202.x.

Liou, K. N. (2002), *An Introduction to Atmospheric Radiation*, 583 pp., Elsevier, New York.

Lloyd, J., et al. (2001), Vertical profiles, boundary layer budgets, and regional flux estimates for CO_2 and its $^{13}C/^{12}C$ ratio and for water vapor above a forest/bog mosaic in central Siberia, *Glob. Biogeochem. Cycles*, *15*(2), 267–284.

Michalakes, J., S. Chen, J. Dudhia, L. Hart, J. Klemp, J. Middlecoff, and W. Skamarock (2001), Development of a next generation regional weather research and forecast model, in *Developments in Teracomputing: Proceedings of the Ninth ECMWF Workshop on the Use of High Performance Computing in Meteorology*, edited by W. Zwieflhofer and N. Kreitz, pp. 269–276, World Scientific, Hackensack, N. J.

Obukhov, A. M. (1959), Description of turbulence in terms of Lagrangian variables, *Adv. Geophys.*, *6*, 113–116.

Palmer, T., C. Brankovic, R. Buizza, P. Chessa, L. Ferranti, B. Hoskins, and A. Simmons (2000), *A Review of Predictability and ECMWF Forecast Performance, with emphasis on Europe*, European Centre for Medium-Range Weather Forecasts, Reading, UK.

Parlange, M. B., W. E. Eichinger, and J. D. Albertson (1995), Regional scale evaporation and the atmospheric boundary layer, *Rev. Geophys.*, *33*(1), 99–124.

Parrish, D. F., J. C. Derber, R. J. Purser, W. S. Wu, and Z. X. Pu (1997), The NCEP global analysis system: Recent improvements and future plans, *J. Meteorol. Soc. Jpn.*, *75*(1B), 359–365.

Parrish, D. D., M. Trainer, D. Hereid, E. J. Williams, K. J. Olszyna, R. A. Harley, J. F. Meagher, and F. C. Fehsenfeld (2002), Decadal change in carbon monoxide to nitrogen oxide ratio in U.S. vehicular emissions, *J. Geophys. Res.*, *107*(D12), 4140, doi:10.1029/2001JD000720.

Peixoto, J. P., and A. H. Oort (1992), *Physics of Climate*, 520 pp., American Institute of Physics, New York.

R Development Core Team (2004), *A Language and Environment for Statistical Computing* (www.r-project.org), R Foundation for Statistical Computing, Vienna, Austria.

Rabier, E., H. Jarvinen, E. Klinker, J. F. Mahfouf, and A. Simmons (2000), The ECMWF operational implementation of four-dimensional variational assimilation: I. Experimental results with simplified physics, *Q. J. R. Meteorol. Soc.*, *126*(564), 1143–1170.

Rodean, H. C. (1996), *Stochastic Lagrangian Models of Turbulent Diffusion*, 84 pp., Am. Meteorol. Soc., Boston, Mass.

Rolph, G. D. (2003), *Real-time Environmental Applications and Display system* (READY) (http://www.arl.noaa.gov/ready/hysplit4.html), NOAA Air Resources Laboratory, Silver Spring, Md.

Schmitgen, S., H. Geib, P. Ciais, B. Neininger, Y. Brunet, M. Reichstein, D. Kley, and A. Volz-Thomas (2004), Carbon dioxide uptake of a forested region in southwest France derived from airborne CO2 and CO measurements in a quasi-Lagrangian experiment, *J. Geophys. Res.*, *109*(D14), D14302, doi:10.1029/2003JD004335.

Schwartz, B. E., and M. Govett (1992), *A hydrostatically Consistent North American Radiosonde Data Base at the Forecast Systems Laboratory, 1946–Present*, NOAA Technical Memorandum ERL FSL-4, NOAA FSL, Boulder, Colo.

Smith, F. B. (1968), Conditioned particle motion in a homogeneous turbulent field, *Atmos. Environ.*, *2*, 491–508.

Stohl, A. (1998), Computation, accuracy and applications of trajectories—A review and bibliography, *Atmos. Environ.*, *32*(6), 947–966.

Stohl, A., et al. (2003), A backward modeling study of intercontinental pollution transport using aircraft measurements, *J. Geophys. Res.*, *108*(D12), 4370, doi:10.1029/2002JD002862.

Stohl, A., O. R. Cooper, R. Damoah, F. C. Fehsenfeld, C. Forster, E. Y. Hsie, G. Hubler, D. D. Parrish, and M. Trainer (2004), Forecasting for a Lagrangian aircraft campaign, *Atmos. Chem. Phys.*, *4*, 1113–1124.

Stokes, G. M., and S. E. Schwartz (1994), The Atmospheric Radiation Measurement (ARM) program—Programmatic background and design of the cloud and radiation test bed, *Bull. Am. Meteorol. Soc.*, *75*(7), 1201–1221.

Straume, A. G., E. N. D. Koffi, and K. Nodop (1998), Dispersion modeling using ensemble forecasts compared to ETEX measurements, *J. Appl. Meteorol.*, *37*, 1444–1456.

Stull, R. B. (1988), *An Introduction to Boundary Layer Meteorology*, 666 pp., Springer, New York.

Thompson, A. M., K. E. Pickering, R. R. Dickerson, W. G. Ellis, D. J. Jacob, J. R. Scala, W. K. Tao, D. P. McNamara, and J. Simpson (1994), Convective-transport over the central United States and its role in regional CO and ozone budgets, *J. Geophys. Res.*, *99*(D9), 18,703–18,711.

Uliasz, M., and R. A. Pielke (1990), Receptor-oriented Lagrangian-Eulerian model of mesoscale air pollution dispersion, in *Computer Techniques in Environmental Studies*, edited by P. Zannetti, pp. 57–68, Comput. Mech., Billerica, Mass.

Wofsy, S. C., and R. C. Harriss (2002), *The North American Carbon Program (NACP), NACP Committee of the U.S. Interagency Carbon Cycle Science Program*, U.S. Global Change Research Program, Washington, D. C.

Wofsy, S. C., M. L. Goulden, J. W. Munger, S.-M. Fan, P. S. Bakwin, B. C. Daube, S. L. Bassow, and F. A. Bazzaz (1993), Net exchange of CO2 in a mid-latitude forest, *Science*, *260*, 1314–1317.

V. Y. Chow, B. C. Daube, E. Gottlieb, D. M. Matross, and S. C. Wofsy, Department of Earth and Planetary Sciences, Harvard University, Cambridge, MA, USA.

C. Gerbig, Max-Planck-Institut für Biogeochemie, Jena, Germany.

J. C. Lin, Department of Earth and Environmental Sciences, University of Waterloo, Waterloo, Ontario, Canada. (jcl@uwaterloo.ca)